Bull. Astr. Soc. India (2002) 30, 193–199

Electrodynamic Structure of an Outer–Gap Accelerator: Gamma-Ray Emission from the Crab Pulsar

Kouichi HIROTANI[1] and Shinpei SHIBATA[2]

[1] *NASA/Goddard Space Flight Center, Greenbelt, MD 20771, USA*
[2] *Department of Physics, Yamagata University, Yamagata 990-8560, Japan*

Abstract. We investigate a stationary pair production cascade in the outer magnetosphere of a spinning neutron star. The charge depletion due to a global current, causes a large electric field along the magnetic field lines. Migratory electrons and/or positrons are accelerated by this field to radiate curvature gamma-rays, some of which collide with the X-rays to materialize as pairs in the gap. The replenished charges partially screen the electric field, which is self-consistently solved together with the distribution functions of particles and gamma-rays. If no current is injected at either of the boundaries of the accelerator, the gap is located around the conventional null surface, where the local Goldreich-Julian charge density vanishes. However, we first find that the gap position shifts outwards (or inwards) when particles are injected at the inner (or outer) boundary. Applying the theory to the Crab pulsar, we demonstrate that the pulsed TeV flux does not exceed the observational upper limit for moderate infrared photon density and that the gap should be located near to or outside of the conventional null surface so that the observed spectrum of pulsed GeV fluxes may be emitted via a curvature process.

Key words: gamma-ray observations, gamma-ray theories, individual pulsar (Crab)

1. Introduction

The EGRET experiment on the Compton Gamma Ray Observatory has detected pulsed signals from seven rotation-powered pulsars (e.g., for Crab, Nolan et al. 1993, Fierro et al. 1998). The modulation of the γ-ray light curves at GeV energies testifies to the production of γ-ray radiation in the pulsar magnetospheres either at the polar cap (Harding, Tademaru, & Esposito 1978; Daugherty & Harding 1982, 1996), or at the vacuum gaps in the outer magnetosphere (Cheng, Ho, & Ruderman 1986a,b, hereafter CHR;

Romani 1996; Zhang & Cheng 1997). Effective γ-ray production in a pulsar magnetosphere may be extended to the very high energy (VHE) region above 100 GeV as well. If the VHE emission originates the pulsar magnetosphere, a significant fraction of them can be expected to show pulsation. However, only the upper limits have been obtained for pulsed TeV radiation (e.g., Hillas et al. 1998; Lessard et al. 2000). Therefore, the lack of pulsed TeV emissions provides a severe constraint on the modeling of particle acceleration zones in a pulsar magnetosphere. For example, in the CHR picture, the magnetosphere should be optically thick for pair-production in order to reduce the TeV flux to an unobserved level by absorption. This in turn requires very high luminosities of infrared photons. However, the required IR fluxes are generally orders of magnitude larger than the observed values (Usov 1994). We are therefore motivated by the need to contrive an outer-gap model which produces less TeV emission with a moderate infrared luminosity.

High-energy emission from a pulsar magnetosphere, in fact, crucially depends on the acceleration electric field, $E_\parallel$, along the magnetic field lines. It was Hirotani and Shibata (1999, hereafter Papers I, II, III), and Hirotani (2000a,b, Paper IV,VI; 2001, Paper V) who first considered the spatial distribution of $E_\parallel$ together with particle and γ-ray distribution functions. By solving the Vlasov equations, they demonstrated that a stationary gap is formed around the conventional null surface at which the local Goldreich-Julian charge density,

$$\rho_{\rm GJ} = -\frac{\Omega B_z}{2\pi c}, \tag{1}$$

vanishes, where B_z is the component of the magnetic field along the rotation axis, Ω the angular frequency of the neutron star, and c the speed of light.

In the next section, we formulate the pair-production cascade. We then apply the theory to the Crab pulsar and present the expected γ-ray spectra in § 3.

2. Basic Equations and Boundary Conditions

Let us first consider the Poission equation for the electrostatic potential, Φ. Neglecting relativistic effects, and assuming that typical transfield thickness of the gap, $D_\perp$, is greater than or comparable with the longitudinal gap width, W, we can reduce the Poisson equation into the one-dimensional form (Paper VI)

$$E_\parallel = -\frac{d\Phi}{ds}, \qquad \frac{dE_\parallel}{ds} = 4\pi e\left(N_+ - N_- - \frac{\rho_{\rm GJ}}{e}\right) \tag{2}$$

where N_+ and N_- designate the positronic and electronic densities, respectively, e the magnitude of the charge on an electron, and s the length along the last-open fieldline.

We next consider the continuity equations for the particles. Assuming that both electrostatic and curvature-radiation-reaction forces cancel out each other, we obtain the following continuity equations

$$\pm B\frac{d}{ds}\left(\frac{N_\pm}{B}\right) = \frac{1}{c}\int_0^\infty d\epsilon_\gamma\,[\eta_{\rm p+}G_+ + \eta_{\rm p-}G_-], \tag{3}$$

where $G_{\pm}(s, \epsilon_\gamma)$ are the distribution functions of γ-ray photons having momentum $\pm m_e c \epsilon_\gamma$ along the poloidal field line. Since the electric field is assumed to be positive in the gap, e^+'s (or e^-'s) migrate outwards (or inwards). The pair production redistribution functions, $\eta_{p\pm}$, are defined as

$$\eta_{p\pm}(\epsilon_\gamma) = (1 - \mu_c)\frac{c}{\omega_p}\int_{\epsilon_{th}}^{\infty} d\epsilon_x \frac{dN_x}{d\epsilon_x}\sigma_p(\epsilon_\gamma, \epsilon_x, \mu_c), \tag{4}$$

where σ_p is the pair-production cross section and $\cos^{-1}\mu_c$ refers to the collision angle between the γ-rays and the X-rays.

A combination of equations (3) gives the current conservation law,

$$\frac{\Omega}{2\pi} j_{tot} \equiv ce[N_+(s) + N_-(s)] = \text{constant for } s. \tag{5}$$

When $j_{tot} = 1.0$, the current density per unit flux tube equals the Goldreich–Julian value, $\Omega/(2\pi)$.

Assuming that the outwardly (or inwardly) propagating γ-rays dilate (or constrict) at the same rate with the magnetic field, we obtain (Paper VI)

$$\pm B\frac{\partial}{\partial s}\left(\frac{G_\pm}{B}\right) = -\frac{\eta_{p\pm}}{c}G_\pm + \frac{\eta_c}{c}N_\pm, \tag{6}$$

where η_c is explicitly defined by equations (49)–(50) in Paper VI.

We impose the following boundary conditions at the *inner* (starward) boundary ($s = s_1$):

$$E_\parallel(s_1) = 0, \quad \Phi(s_1) = 0, \quad G_+(s, \epsilon_\gamma) = 0, \quad \text{and} \quad N_+(s) = \frac{\Omega}{2\pi ce} j_1. \tag{7}$$

The last condition yields $N_-(s_1) = (\Omega/2\pi ce)(j_{tot} - j_1)$.

At the *outer* boundary ($s = s_2$), we impose

$$E_\parallel(s_2) = 0, \quad G_-(s_2, \epsilon_\gamma) = 0, \quad \text{and} \quad N_-(s_2) = \frac{\Omega}{2\pi ce} j_2. \tag{8}$$

The current density created in the gap is expressed as $j_{gap} = j_{tot} - j_1 - j_2$. We adopt j_{gap}, j_1, and j_2 as the free parameters.

Dividing the γ-ray energies into m bins, we obtain totally $6+2m$ boundary conditions for $4 + 2m$ unknowns. Thus two extra boundary conditions must be compensated by making the positions of the boundaries s_1 and s_2 be free. The two free boundaries appear because $E_\parallel = 0$ is imposed at *both* the boundaries and because j_{gap} is externally imposed. In other words, the gap boundaries shift, if j_1 and/or j_2 varies.

3. Application to the Crab Pulsar

In this section, we apply the theory to the Crab pulsar. The rotational frequency and the magnetic moment are $\Omega = 188.1$ rad s^{-1} and $\mu = 3.38 \times 10^{30}$ G cm^3. HEAO 1 observations revealed that the X-ray spectrum in the primary pulse phase is expressed by

$$\frac{dN_{\rm pl}}{d\epsilon_{\rm x}} = N_{\rm pl}\epsilon_{\rm x}{}^{\alpha} \quad (\epsilon_{\rm min} < \epsilon_{\rm x} < \epsilon_{\rm max}), \tag{9}$$

with $\alpha = -1.81$ and $N_{\rm pl} = 5.3 \times 10^{15} d^2 (r_0/\varpi_{\rm LC})^{-2}$ (Knight 1982), where d refers to the distance in kpc. We adopt $\epsilon_{\rm min} = 0.1$ keV /511 keV and $\epsilon_{\rm max} = 50$ keV /511 keV. Substituting this power-law spectrum into equation (4), we can solve the Vlasov equations by the method described in § 2.

To reveal the spatial distribution of the acceleration field, we consider the following four representative boundary conditions:

case 1 $(j_1, j_2) = (0, 0)$,
case 2 $(j_1, j_2) = (0.25, 0)$,
case 3 $(j_1, j_2) = (0.5, 0)$,
case 4 $(j_1, j_2) = (0, 0.25)$.

That is, for case 2 (or case 4), the positronic (or electronic) current flowing into the gap per unit flux tube at the inner (or outer) boundary is 25% of the typical Goldreich-Julian value, $\Omega/2\pi$. We fix $j_{\rm gap} = 0.01$ for all the four cases, because the solution forms a 'brim' to disappear (fig. 2 in Hirotani & Okamoto 1998) if $j_{\rm gap}$ exceeds a few percent. In what follows, we adopt 45° as the magnetic inclination, which is necessary to compute B at each point for the Newtonian dipole field.

The results of $E_{\parallel}(\xi)$ for the four cases are presented in figure 1. The abscissa designates the distance along the last-open field line and covers the range from $s = 0$ (neutron star surface) to $s = 1.2\varpi_{\rm LC} = 1.91 \times 10^6$ m. The solid curve (case 1) shows that the gap is located around the conventional null surface. However, the gap shifts outwards as j_1 increases, as the dashed (case 2) and dash-dotted (case 3) curves indicate. On the other hand, when j_2 increases, the gap shifts inwards and the potential drop, $\Psi(s_2)$, reduces significantly. For example, we obtain $\Psi(s_2) = 7.1 \times 10^{12}$ V for case 4, whereas 1.7×10^{13} V for case 2.

Let us now consider the GeV and TeV emission from the gap. The GeV spectra is readily computed from the solved $G_{\pm}$. The TeV spectra is, on the other hand, obtained by inputting some infrared spectrum. Because the pulsed flux around eV energies are difficult to be observed, we assume that the IR spectrum below $\epsilon_{\rm IR} < 10^{-6}$ (or equivalently, below 1.23×10^{14} Hz) becomes optically thick for synchrotron self-absorption and adopt $\alpha = 1.5$. Setting $F_\nu = 3$ mJy at $\epsilon_{\rm IR} = 10^{-6}$, which is consistent with near-IR and optical observations (Eikenberry et al. 1997), we obtain $N_0 = 2.3 \times 10^{32}$cm^{-3}, where

$$\frac{dN_{\rm IR}}{d\epsilon_{\rm IR}} = N_0 \epsilon_{\rm IR}^{\alpha}; \tag{10}$$

$\epsilon_{\rm IR} m_{\rm e} c^2$ refers to the IR photon energy. Using this IR spectrum, we can compute the spectrum of the upscattered photons by the method described in § 4.4 in Paper V. It is

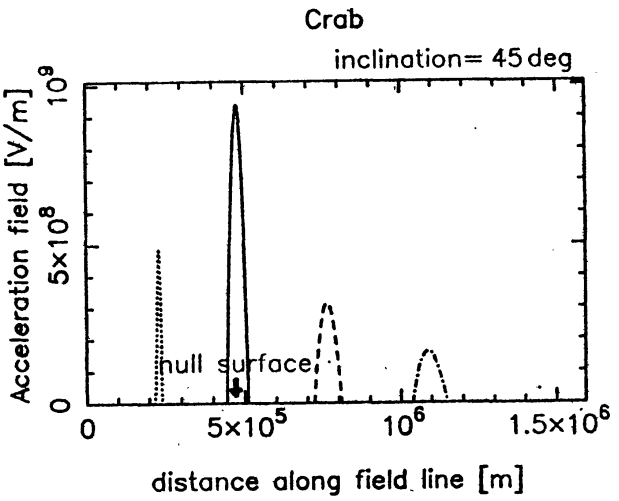

Figure 1. Distribution of $E_{\parallel}(s)$; the abscissa is in meters. The solid, dashed, dash-dotted, and dotted curves correspond to the cases 1, 2, 3, and 4, respectively (see text).

noteworthy that the optical depth for the TeV photons to be absorbed by the same IR field is about 5 for the Crab pulsar (§ 4.2 in Hirotani & Shibata 2001a, Paper VII).

We present the γ-ray spectra for the four cases in figure 2 (see also Paper VII), multiplying the cross sectional area of $D_\perp{}^2 = (6W)^2$. If $D_\perp$ increase twice, both the GeV and TeV fluxes increases four times. In GeV energies, the observational pulsed spectrum is obtained by EGRET observations (open circles; Nolan et al. 1993), while in TeV energies, only the upper limits are obtained by Whipple observations (open squares; Weekes et al. 1989; Reynolds et al. 1993; Goret et al. 1993; Hillas, A. M.; Lessard et al. 2000), Durham observations (open triangle; Dowthwaite et al. 1984), and CELESTE observations (open square at 60 GeV; Holder, J., private communication). The filled circles denote the unpulsed flux obtained by CANGAROO observations (Tanimori et al. 1998).

It follows from figure 2 that the TeV flux is undetectable except for $h\nu \sim 10$ TeV. Around 10 TeV, the γ-ray flux is slightly less than or comparable with the observational upper limits for cases 1, 2, and 3, and exceeds the limits for case 4. Nevertheless, we can exclude case 4 from consideration, because the expected GeV spectrum is very very soft and is inconsistent with the EGRET observations, whatever $D_\perp$ we may assume.

It is noteworthy that the GeV spectrum, which does not depend on the assumed IR field, depends on j_1 and j_2 significantly. In particular, in case 4 (as the dotted curves show), the GeV emission significantly decreases and softens, because both the potential drop and the maximum of $E_{\parallel}$ reduce as the gap shifts inwards. As a result, it becomes impossible to explain the EGRET spectrum around 10 GeV, if the gap is located well inside of the conventional null surface.

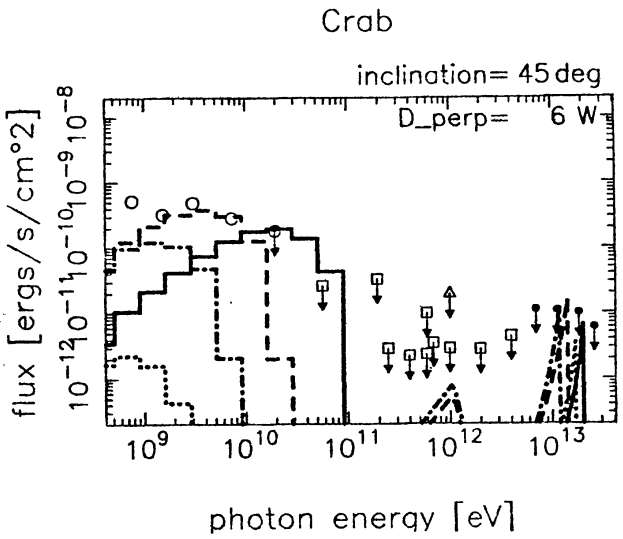

Figure 2. Gamma-ray spectra from the Crab pulsar magnetosphere. The solid, dashed, dash-dotted, and dotted lines correspond to the same cases as in figure 1. For cases 1, 2, and 3, the spectra of the outwardly propagating γ-rays are depicted, because the outward flux dominates the inward one in each case. On the other hand, for case 4, the inwardly propagating γ-ray flux is depicted, because it dominates the outerwad one.

To sum up, we have developed a one-dimensional model for an outer-gap accelerator in the magnetosphere of a rotation-powered pulsar. When a magnetospheric current flows into the gap from the outer (or inner) boundary, the gap shifts inwards (or outwards). In particular, when a good fraction of the Goldreich-Julian current density is injected from the outer boundary, the gap is located well inside of the conventional null surface; the resultant GeV emission becomes very soft and weak. These conclusions are, in general, consistent with those obtained for other pulsars (Hirotani & Shibata 2001b, Paper VIII). Applying this method to the Crab pulsar, we find that the gap should be located near to or outside of the conventional null surface, so that the observed GeV spectrum of pulsed GeV fluxes may be emitted via curvature process. By virtue of the absorption by the dense IR field in the magnetosphere, the problem of excessive TeV emission does not arise in our outer-gap calculation.

References

Cheng, K. S., Ho, C. and Ruderman, M., 1986a ApJ, 300, 500.
Cheng, K. S., Ho, C. and Ruderman, M., 1986b ApJ, 300, 522.
Daugherty, J. K. and Harding, A. K. 1982, ApJ, 252, 337
Eikenberry, S. S., Fazio, G. G., Ransom, S. M., Middleditch, J., Kristaian, J. and Pennypacker, C. R. 1997, ApJ 477, 465
Fierro, J. M., Michelson, P. F., Nolan, P. L. and Thompson, D. J., 1998, ApJ 494, 734
Harding, A. K., Tademaru, E. and Esposito, L. S. 1978, ApJ, 225, 226
Hillas, A. M., Akerlof, C. W., Biller, S. D., Buckley, J. H., Carter-Lewis, D. A., Catanese, M., Cawley, M. F., Fegan, D. J. et al. 1998, ApJ 503, 744.

Hirotani, K., 2000a PASJ 52, 645 (Paper VI).
Hirotani, K., 2000b, MNRAS 317, 225 (Paper IV).
Hirotani, K., 2001, ApJ 549, 495 (Paper V).
Hirotani, K. and Okamoto, I., 1998, ApJ, 497, 563.
Hirotani, K. and Shibata, S., 1999a, MNRAS 308, 54 (Paper I).
Hirotani, K. and Shibata, S., 1999b, MNRAS 308, 67 (Paper II).
Hirotani, K. and Shibata, S., 1999c, PASJ 51, 683 (Paper III).
Hirotani, K. and Shibata, S., 2001a, ApJ in press (Paper VII, astro-ph/0101498).
Hirotani, K. and Shibata, S., 2001b, MNRAS in press (Paper VIII, astro-ph/0012062).
Knight, F. K., 1982, ApJ 260, 538.
Lessard, R. W., Bond, I. H., Bradbury, S. M., Buckley, J. H., Burdett, A. M., Carter-Lewis, D. A. Catanese, M. Cawley, M. F., et al. 2000, ApJ 531, 942
Moffett, D. A., Hankins, T. H. 1996, ApJ 468, 779
Nolan, P. L., Arzoumanian, Z., Bertsch, D. L., Chiang, J., Fichtel, C. E., Fierro, J. M., Hartman, R. C., Hunter, S. D., et al. 1993, ApJ 409, 697
Percival, J. W., et al. 1993, ApJ 407, 276
Romani, R. W., 1996, ApJ 470, 469.
Usov, V. V. 1994, ApJ 427, 394
Zhang, L. Cheng, and K. S. 1997, ApJ 487, 370.